Chemical Papers
https://doi.org/10.1007/s11696-022-02236-7

ORIGINAL PAPER

Green starch/graphene oxide hydrogel nanocomposites for sustained release applications

Asmaa Sayed[1] · Mai Yasser[2] · Manar El-sayed Abdel-raouf[3] · Reham Mohsen[2,4]

Received: 10 November 2021 / Accepted: 15 April 2022

Abstract

Green nanocomposite hydrogels (ST-PHEMA/GO) comprised of starch and 2-Hydroxyethyl methacrylate (HEMA) reinforced with different ratios of graphene oxide (GO) were prepared via gamma radiation induced crosslinking polymerization. The chemical structure and morphology and the crystallinity were studied by FTIR FE-SEM, AFM, TEM and XRD, respectively. The swelling behavior of the claimed hydrogels was verified versus time and the pH-dependent swelling at three different irradiation dose:10, 20 and 30 kGy was also investigated. The results of the swelling study showed that the swelling capacity of the hydrogel networks varied with the changes of the pH of the solution, the GO content and the irradiation doses. Moreover, the swelling isotherm of all the prepared hydrogels followed a Fickian diffusion mechanism $n < 0.5$.

Graphical abstract

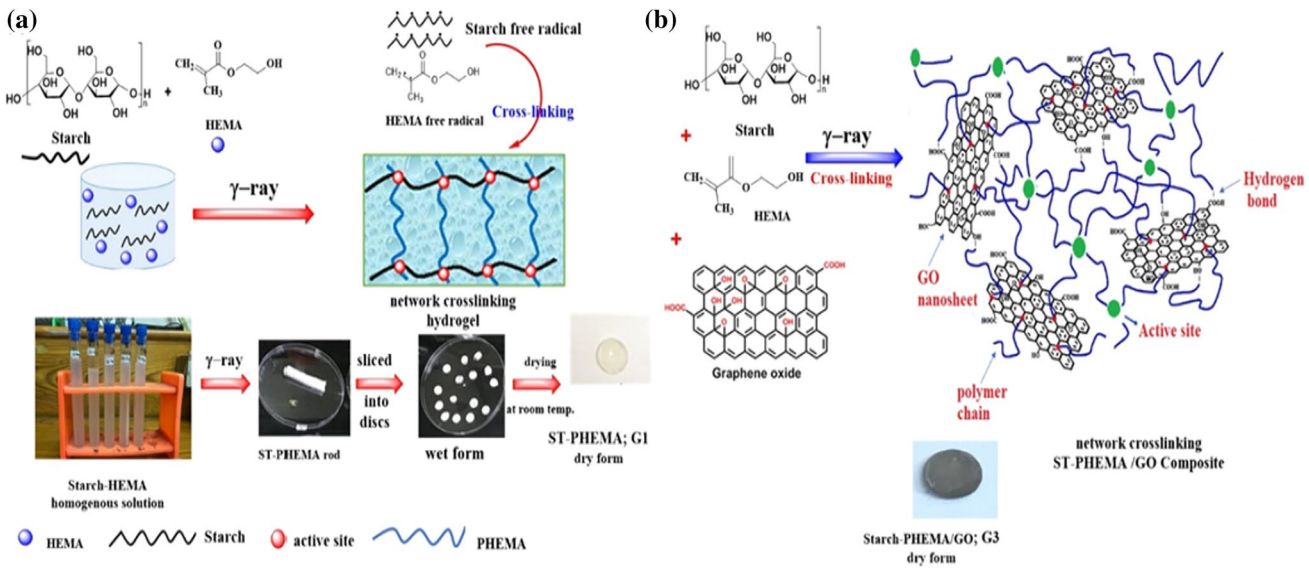

Keywords Biopolymer · Gamma-irradiation · Polymerization · Characterization · Atomic force microscopy · Swelling study

Introduction

Investigating the properties of natural polymers such as their biocompatibility (Rattanawongwiboon et al. 2020; Arican et al. 2021), renewability, biodegradability (Ansari et al. 2021) and toxicity profiles has shed the light on their

✉ Asmaa Sayed
asmaasayedncrrt@gmail.com

Extended author information available on the last page of the article

Published online: 10 May 2022

reputation in several fields (Konstantakos et al. 2019; Chin et al. 2019; Harish Kumar et al. 2019a, b). Starch is one of the most plentiful carbohydrates in nature, comprising D-glucopyranose polymers linked by α-1,4 and α-1,6 glycosidic bonds (Maji 2019). As a natural polymer, starch is inexpensive, biodegradable and renewable, thus encouraged researchers to investigate its possible use in different applications (Yu et al. 2017; Mishra et al. 2018). 2-Hydroxyethyl methacrylate (HEMA) was less harmful to the human body than any other acrylates employed used in the biomedical field (Wang et al. 2013). *Wöhl-Bruhn and coworkers* prepared crosslinked polymers based on modified hydroxyethyl starch (HES) using hydroxyethyl methacrylate (HEMA), and the results have exhibited the ability of HES derivatization with different degrees of substitution (DS) to produce (HES-HEMA) a photo-cross linkable polymer (Wöhl-Bruhn et al. 2012). Starch has been combined with acrylamide and HEMA copolymer hydrogel crosslinked with N–N′ methylenebisacrylamide (MBA) with various ratios of crosslinker and comonomer forming semi-interpenetrating network hydrogel with high swelling properties that was employed for water treatment in adsorbing industrials dyes, such as methyl violet and malachite green (Bhattacharyya and Ray 2014). On the other hand, Graphene is a nanomaterial with hexagonal conjugated structure, comprising one atom thick sheet of carbon in a two-dimensional shape. It was first used in 2004 in optoelectronic and mechanical fields and lately, its applications are potent in the biomedical field as studies demonstrated that graphene can affect cell growth and differentiation (Han et al. 2011). Graphene oxide (GO) is graphene derivative that possesses numerous oxygen-containing functional groups, including carboxylic (–COOH), carbonyl (C=O) and hydroxyl (–OH) (Krishnamoorthy et al. 2013; Papageorgiou et al. 2017) amenable to modification using radiation-induced graft copolymerization (Singh and Singh 2020). Even if a small amount is added, GO can still enhance polymer physical properties (Abbasian et al. 2018) because of its large surface area, excellent dispersion in water and other aqueous media via hydrogen bonding formation and electrostatic interactions within polymers (Miao et al. 2013; Rasoulzadehzali and Namazi 2018; Naicker et al. 2020). Grafting of GO onto polymer matrix leads to polymer nanocomposites used for sensors applications, metal ion adsorption, in addition to wound dressings and drug delivery systems (Qi et al. 2019; Arshad et al. 2019; Ali et al. 2019). The surface of GO can also help cells adhere and proliferate, and its antibacterial properties can preclude risk of inflammatory processes (Parveen Kumar et al. 2019a, b). Several authors have investigated the biosafety of graphene oxide-based nanocomposite polymers as antibacterial materials. For instance, *Yang and colleagues* (Yang et al. 2018) fabricated poly (vinyl alcohol)-chitosan/graphene oxide (PVA-CS/GO) composite nanofibers through electrospinning and manifested remarkable antibacterial activity towards E. coli and S. aureus. *Huang and coworkers* (Huang et al. 2015) prepared GO-polyethyleneimine hybrid films, exhibiting improved mechanical strength and displaying good antibacterial activity. Recently, several studies have been carried out using GO to develop drug delivery systems (Liu et al. 2014; Rao et al. 2018; Parveen Kumar et al. 2019a, b). *Pereira* et al. have reported that using in-situ polymerization to incorporate graphene oxide into PHEMA matrix led to highly cytocompatible hydrogels, opening up a broad spectrum of biotechnological implementations (Pereira et al. 2019). Compared to chemical methods, preparing copolymers by radiation-induced graft copolymerization is a clean, convenient and inexpensive method (Sayed et al. 2022). Therefore, gamma irradiation is generally regarded as a viable approach to design biomedical polymers. Hence, the objectives of the present study are to prepare green starch based-graphene oxide nanocomposites via gamma irradiation induced copolymerization and crosslinking as a new eco-friendly biopolymer, introduce full description of the structural, morphological, and physicochemical characteristics of obtained (ST-PHEMA/GO) hydrogel nanocomposites via different tools. Then, investigating the swelling behavior of the claimed hydrogels at different pH values to prove the applicability of the hydrogel nanocomposites as smart pH responsive candidates for sustained release. Finally, correlating the data with structural features to monitor the effect of graphene oxide on the properties and the pertinence of the demanded hydrogel nanocomposites.

Experimental

Chemicals

Native starch powder (ST) was purchased from Al-Nasr company for chemical industries as ultra pure white dry powder, **Hydroxyethyl methacrylate (HEMA)** was supplied from Merck, Darmstadt, Germany, **Graphene Oxide (GO)** was purchased from Acmatic, Cairo, Egypt (average size length 1–3 µm and thickness 1–5 nm). Deionized water was used in all the preparations and all the solvents were used as reagent grade solvents.

2.2. Preparation of (ST-PHEMA) hydrogel

A fixed optimized ratio of starch to HEMA (1:3) was applied according to a previous work in order to gratify proper gelation with controlled swelling and sustained release (Mahmoud et al. 2014). Simply, Starch (5 wt%) was dissolved in 85 ml deionized water and stirred at 60 °C until gelatinization. Then, 15 mL of HEMA monomer was added to the gelatinized starch solution then the solution was

stirred at ambient temperature until complete homogenity, where the total polymer and monomer content was 20 wt%. Then, 20 mL of the resulted solution was poured into three glass test tubes each then they exposed to ^{60}Co-gamma irradiation of irradiation doses 10; 20 and 30 kGy; refered as *ST-PHEMAa, ST-PHEMAb and ST-PHEMAc* respectively. The hydrogels produced were sliced into almost identical discs. To eliminate the unreacted monomer; the hydrogels were incubated overnight in distilled water at 80 °C, then dried in air.

2.3. Preparation of ST-PHEMA/GO nanocomposite

The ratio of graphene oxide in the hydrogel was varied to verify the optimum ratio at which a consistent gel is formed. Graphene oxide solution (0.05gm in 100 mL of deionized water) was sonicated at 25 °C for 30 min then 2 mL isopropyl alcohol was added as a hydroxyl radicals' grubber. Different volumes of GO solution were added to ST-HEMA solution with continuous stirring. The resulted solutions were then transferred into glass test tubes and subjected to ^{60}Co -gamma rays at different irradiation doses 10; 20 and 30 kGy for synthesis of the ST-PHEMA/GO hydrogel nanocomposites.

The code system for the prepared samples is as following, Table 1; ST-PHEMA denotes the hydrogel without GO prepared; the irradiation doses are denoted as a, b and c for 10; 20 and 30 kGy respectively and the nanocomposites are denoted as ST-PHEMA/GO and the numbers from 1–3 refer to the amount of GO solution with respect to the ST-HEMA solution.

2.4. Cracterization of the nanocomposite hydrogels

Fourier transform infrared spectroscopy (FT-IR)

The IR spectra of ST-PHEMA hydrogel and ST-PHEMA/GO were recorded on FT-IR model Bruker, Unicom infrared spectrophotometer, Germany, at 400–4000 cm^{-1} wavelength range.

X–ray diffraction analysis (XRD)

The crystallinity of ST-PHEMA hydrogel and ST-PHEMA/GO nanocomposite samples were examined at room temperature by XD-DI Series, Shimadzu device containing copper target with (λ = 1.542 Å), 30 mA electric current, 40 kV operating voltage, over 2θ of range 4° to 90° and speed of scanning 8°/min to measure the X–Ray Diffraction (XRD) patterns of the samples. The characteristic interplanar distance d is given by the Bragg's Eq. (1)(Todica 2015):

$$d = \frac{K.\lambda}{2\sin\sin\theta} \quad (1)$$

where, K is the diffraction order, θ is the diffraction angle and λ (1.54 A°) is the wavelength of monochromatic X–ray beam radiation.

The size of the ordered domains L_θ was calculated by Debye–Scherrer Eq. (2)

$$L_\theta = \frac{k.\lambda}{\beta\cos\cos\theta} \quad (2)$$

where, β denotes the full width at half maximum (FWHM) for corresponding diffraction peak and k is constant (0.9–1).

Field emission scanning electron microscopy (FE-SEM)

The morphology of nanocomposites surface (ST-PHEMA/GO) was examined by a high-resolution electron microscope (SEM) (JEOL—JSM 5200 SCANNING MICROSCOPE, Japan) with voltage accelerated at 25 kV.

Atomic force microscopy (AFM)

The topography of some hydrogels and hydrogel nanocomposites was monitored via the AFM, Flexaxiom Nanosurf, C3000 at the dynamic mode (non-contact) to confirm chemical modification and to detect the changes accompanying the swelling process. The AFM measurements were conducted at room temperature using a NCLR rectangular -shaped silicon cantilever with a resonant frequency of 9 kHz.

Table 1 The composition of different hydrogel/hydrogel nanocomposite samples

Code	Irradiation dose (kGy)						Remarks
	10 (a)		20 (b)		30 (c)		
	ST-HEMA (mL)	GO (mL)	ST-HEMA (mL)	GO (mL)	ST-HEMA (mL)	GO (mL)	
ST-PHEMA	20	0	20	0	20	0	Formation of hydrogel
ST-PHEMA/GO1a-c	19	1	19	1	19	1	Formation of hydrogel
ST-PHEMA/GO2a-c	18	2	18	2	18	2	Formation of hydrogel
ST-PHEMA/GO3a-c	17	3	17	3	17	3	No hydrogel is formed

Transmission electron microscopy (TEM)

The structure of the nanocomposite was observed using transmission electron microscope (TEM) (JEOL—JEM 1400CX ELECTRON MICROSCOPE, Japan,) at acceleration voltage 80 kV. The hydrogel nanocomposites were grinded carefully and dissolved in acetone then sonicted for 5 min. One drop of each solution was deposited on a microgrid of carbon-coated copper grid, to prevent the high-voltage electron beam from damaging the sample; the chamber of the sample inside the device was placed in a bath of liquid nitrogen to stabilize the temperature.

2.5. Swelling study

A sample of ST-PHEMA hydrogel and ST-PHEMA/GO nanocomposite of known weight was submerged in 30 mL distilled water at different time intervals till reaching the equilibrium state to investigate the swelling perfromance verus time. The extra water on the turgid samples surface was eliminated using a filter paper then the samples were reweighed again. Then, the same procedure was repeated at various pH solutions; 2, 3, 5.5, 7.5 and 10.5 to verify the effect of pH on swelling process. The swelling percentage was calculated using the following equation:

$$\text{Degree of Swelling(wt\%)} = \frac{W_t - W_d}{W_d} \times 100 \tag{3}$$

where W_t is the weight of the wet hydrogel at time $''t''$and W_d is weight of dry hydrogel.

Swelling kinetics

The swelling kinetic parameters of ST-PHEMA hydrogel and ST-PHEMA/GO hydrogel nanocomposites were studied in which the mechanism of absorption of water into the hydrogel and nanocomposite voids was known by calculating the equations below:

$$F = \frac{W_t}{W_{eq}} = kt^n \tag{4}$$

$$\ln F = \ln\ln k + n\ln\ln t \tag{5}$$

where F is the fraction of water uptake at time t, k is the diffusion constant (depends on the medium of swelling and the type of the hydrogel), n is the diffusion exponent (transport mechanisms information indicator) and W_t and W_{eq} are weights of the hydrogel at a swelling time $''t''$and at equilibrium state, respectively.

The diffusion coefficient (D) was obtained using the following equation:

$$F = 4\left[\frac{Dt}{\pi h^2}\right]^{1/2} \tag{6}$$

where h is the thickness of the sample.

The constant of the absorption rate (K) is calculated by to following equation:

$$-\ln\ln[1 - F] = Kt + C \tag{7}$$

Results and discussion

Structure and morphology of the nanocomposite

FT-IR spectroscopy

FT-IR analysis was conducted for identifying the structure of prepared ST-PHEMA hydrogel and ST-PHEMA/GO hydrogel nanocomposites. Figure 1a shows the FTIR spectra of ST; ST-PHEMAc hydrogel, ST-PHEMA/GO1c and ST-PHEMA/GO2c nanocomposite; while Fig. 1b gives the FTIR spectra for ST-PHEMA/GO2a-c. FTIR spectrum of pure starch shows that stretching vibrations modes and bending vibrations of intramolecular OH-groups occurred as a broad band around 3283 cm^{-1} and 1643 cm^{-1}, respectively. Also, there is a significant peak at 2925 cm^{-1} ascribed for C–H stretching while C–H wagging appears at (~ 1252 cm^{-1}) as reported elsewhere (Basiak et al. 2018; Sarkar et al. 2020; Lanthong et al. 2006).

FTIR spectrum of ST-PHEMAc hydrogel displays a new characteristic band at 1706 cm^{-1} representative to stretching vibrations of C=O bond of HEMA in the hydrogel matrix (Jeyanthi and Panduranga 1990; Abbasi et al. 2002). Vibrational stretching mode and bending vibrations of intramolecular OH-groups occurred at 3345 cm^{-1} and 1639 cm^{-1}, and such a band shift is due to hydrogen bonding interactions among starch and HEMA (Guo et al. 2010). After constructing ST-HEMA/GO hydrogel nanocomposite, the characteristic peaks of ST-PHEMA hydrogel at 3345, 2937, 1706 and 1639 cm^{-1} are shifted to 3342, 2948, 1708 and 1636 cm^{-1} for ST-PHEMA/GO2b and to 3339, 2955, 1708 and 1631 cm^{-1} for ST-PHEMA/GO2c, due to hydrogen bonding formation between GO, ST and HEMA in composite hydrogels, this assumpltion was also suggested by (Subedi et al. 2019). Such finding also suggested that hydrogen bonds were essential in forming biomaterials (Mandal and Ray 2015; Sivakumar and Rao 2002). It is evident from Fig. 1b that no significant changes are found in characteristic bands of ST-PHEMA/GO2c nanocomposite hydrogel, indicating the stability of starch and PHEMA functional groups.

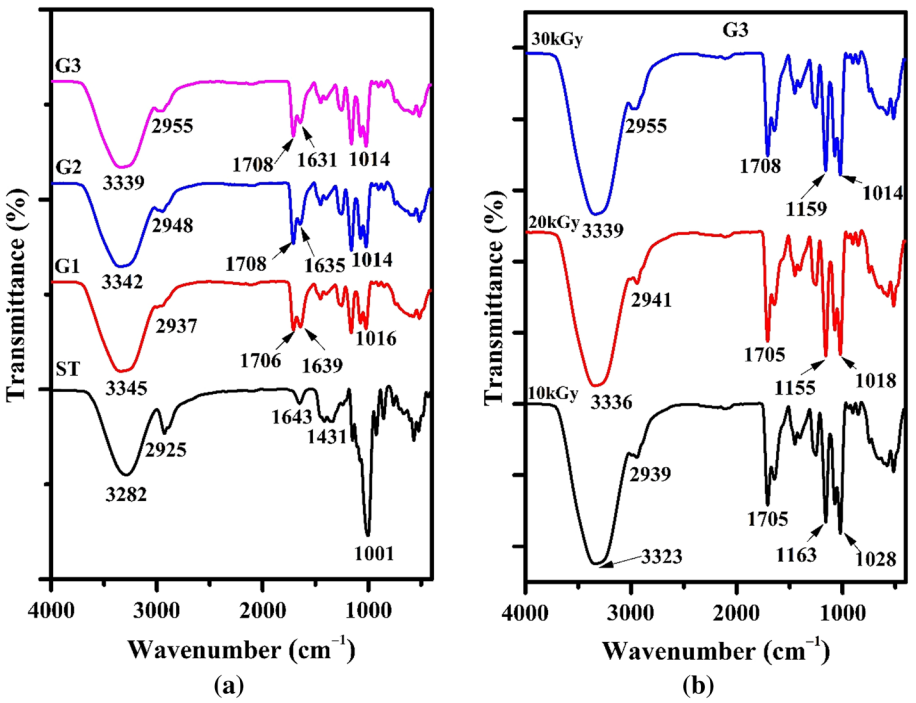

Fig. 1 FTIR Spectra of (a) (1) Neat ST; (2) ST-PHEMAc hydrogel; (3) ST-PHEMA/GO1c and (4) ST-PHEMA/GO2c nanocomposite hydrogels (b) (1) ST-PHEMA/GO2a; (2) ST-PHEMA/GO2b and (3) ST-PHEMA/GO2c nanocomposite hydrogel

Moreover, one can conclude that starch and PHEMA exist in the polymeric network matrix in a non-destructive manner at irradiation doses 10, 20, and 30 kGy.

XRD Analysis

Starch is a semicrystalline material that contains both crystalline (amylose has a linear structure) and amorphous phases (amylopectin has a branched structure) (Haq et al. 2020). The XRD patterns of ST, ST-PHEMAc, and ST-PHEMA/GO1c and ST-PHEMA/GO2c, are demonstrated in Fig. 2a. Starch exhibited main diffraction peaks at 2θ of 6.4°, 13.9° and 16.8° that corresponds to A- or C-type crystal (Fares et al. 2003; Liu et al. 2018). Following grafting starch with HEMA, a broad pattern of XRD without crystalline peak was detected, indicating a decreased crystallinity of ST-PHEMA in comparison with starch, and this may be because of hindrance originated from formed hydrogen bonds between starch chains through HEMA side groups (Haq et al. 2020; Noivoil and Yoksan 2020). In other words, diminishing the intramolecular hydrogen bonding causes a loose packing of starch structure. Similar results were obtained in previous works (Güler et al. 2015; Weerapoprasit and Prachayawarakorn 2019).

The sharp characteristic XRD diffraction peak for the (002) plane of pure GO sheets could be observed at $2\theta = 10.8°$ that corresponds to a *d*-spacing of 0.77 nm. Nevertheless, no characteristic diffraction peak of GO was present in any ST-PHEMA samples, possibly because of too low GO content below the XRD detection limit (Xie et al. 2020) and also GO exfoliation in ST-PHEMA matrix XRD patterns.

The ST-PHEMAc hydrogel exhibited three diffraction peaks at $2\theta = 6.4°$, 13.9°, 16.8°. After incorporation of GO in the ST-PHEMA matrix, the intensive peaks at ~ $2\theta = 13.6°$ and 16.8° appeared again, corresponding to starch crystalline diffraction peak, whereas the intensity of these peaks increased as GO content increases (Fig. 2a) and as irradiation dose increases from 10 to 30 kGy (Fig. 2b) for ST-PHEMA/GO2c. This intensity augmentation of XRD reflections demonstrated more ordered layered structure formation. XRD patterns also exhibited that starch and HEMA produced remarkable interpenetrating copolymeric networks. All the obtained data are summarized in Table 2.

The ratio between the area under the diffraction peak $A_{2\theta}$ (at $2\theta = 16.8°$) to the total area of the entire spectrum A_{tot}, $A_{2\theta}/A_{tot}$, is proportional to the concentration of ordered domains in the sample. The degree of crystallinity of ST-PHEMA increases significantly with increased GO content (from 10.7 for ST-PHEMA/GO2a to 48.0 for ST-PHEMA/GO2c. In addition, as the irradiation dose increases, GO distribution in ST-PHEMA matrix becomes more homogenous. The starch present in the hydrogel matrix in a non-destructive form can illustrate the similarity of interlaminar distance *d* (0.53 nm) at (2θ) 16.80° for all prepared hydrogel.

The structural analyses indicate that degree of ST crystallinity significantly augments with increasing irradiation dose. The size of ordered domains trapped in nanocomposite was determined utilizing Debye Scherrer equation ranging from 8.1 to 10.4 nm.

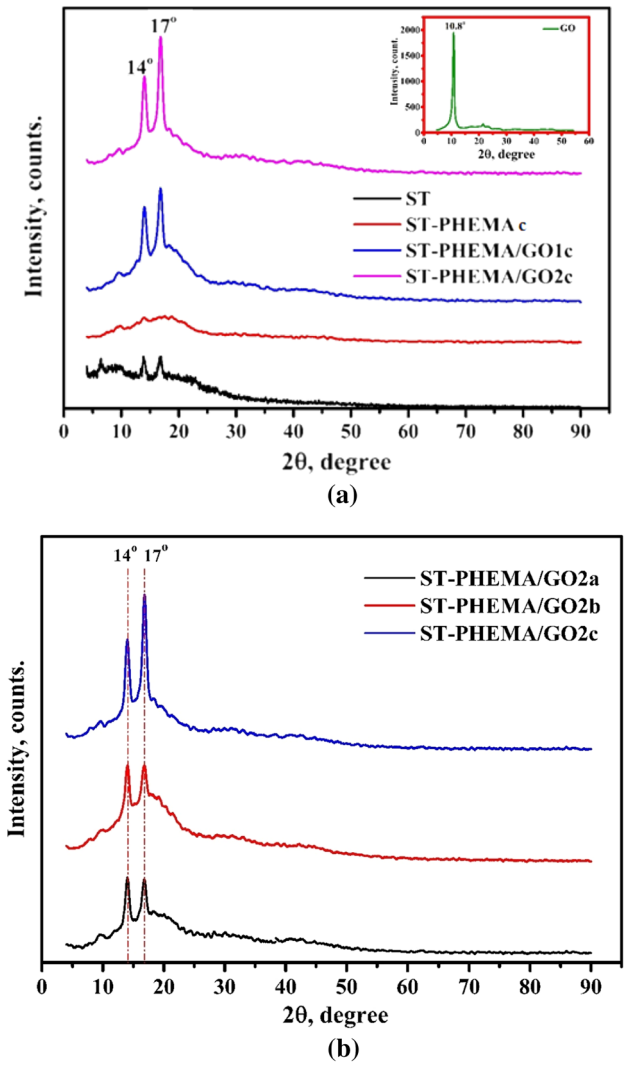

Fig. 2 XRD patterns of (**a**) Neat ST, ST-PHEMAc hydrogel, ST-PHEMA/GO1c and ST-PHEMA/GO2c nanocomposite hydrogels (**b**) ST-PHEMA/GO2a; **b** ST-EMA/GO2b and ST-PHEMA/GO2c nanocomposite hydrogel

Scanning electron microscope (SEM)

The surface morphological characteristics of hydrogel nanocomposites are one of the essential elements that judge the sustained release behavior as well as swelling profile of those hydrogels (Sadeghi 2010; Satish and Shivakumar 2007; Shirin et al. 2019). The surface morphology of ST-PHEMAc, as well as ST-PHEMA/GO2a and ST-PHEMA/GO2c hydrogel nanocomposites were investigated by SEM (Fig. 3a–c respectively).

The SEM image of pure ST-PHEMA hydrogel (Fig. 3a) demonstrates a smooth, uniform porous, and homogeneous morphology. Whereas the images of ST-PHEMA/GO hydrogel nanocomposites (Fig. 3 b and c) display a rough surface with more wrinkles, and the pores disappeared after incorporating GO due to the effective dispersion of GO in ST-PHEMA polymeric matrix. Besides, surface roughness was augmented through incrementing irradiation dose from 10 to 30 kGy. These findings are deemed to be due to severe GO interaction with ST-PHEMA macromolecules as irradiation dose increases. In fact, the interactions between ST, PHEMA, and GO resulted in compressing the network matrix and reducing the porosity, which can restrict the release of encaptured species from ST-PHEMA/GO hydrogel nanocomposite hydrogel. Therefore, we expect that these green composites can be utilized in sustained release applications (Abednejad et al. 2019). In specimens with such a high surface roughness, the post-loading of incorporated species becomes more effective (Saha et al. 2007; Ganguly et al. 2017).

Atomic force microscopy (AFM)

AFM is particularly important in providing more details of the surface features beside other matter properties such as electric and magnetic properties. Some authors used the AFM in polysaccharide characterization by the tapping mode (Chen et al. 2006; Ikeda et al. 2004; Jia et al. 2009). However, in this work, an advanced AFM with wide Z and XY ranges is used to investigate the topographical features and to confirm the chemical modification process and via the AFM, (non-contact, dynamic mode). This was implanted by inspecting three AFM outputs: surface topography, the height represented by the *Z*-axis to measure the difference between the maximum point above the surface and the minimum point below the surface which reflects the porosity and the roughness measurements to monitor physico-chemical changes that occurred to the investigated samples.

Table 2 Crystalline parameters of the prepared ST-PHEMA/GO nanocomposite hydrogel as a function of GO content and irradiation dose at $2\theta = 16.8^{o}$

Sample	*d* [nm]	β [deg.]	Intensity,count	$A_{2\theta}$ [a.u.]	$A_{2\theta}/A_{total}$ [%]	L_{θ}
Neat ST	0.53	0.75	27	1179	27.6	10.7
ST-PHEMAc	0.53	0.77	9	330	10.7	10.4
ST-PHEMA/GO1c	0.53	0.9	71	6277	40.0	8.9
ST-PHEMA/GO2a	0.53	0.92	59	3989	38.5	9.44
ST-PHEMA/GO2b	0.53	0.85	114	7329	42.6	8.7
ST-PHEMA/GO2c	0.53	0.99	152	7657	48.0	8.1

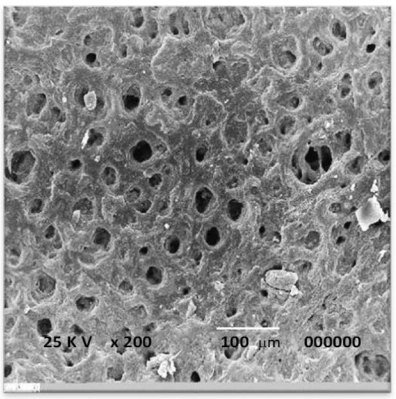

(a) ST-PHEMAc

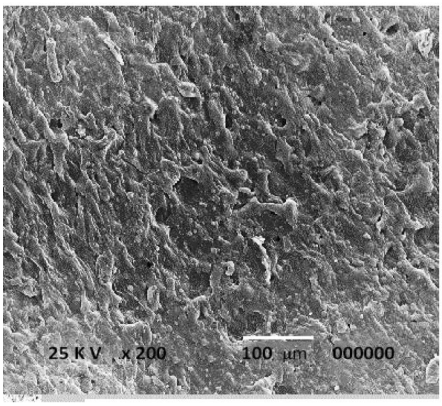

(b) ST-PHEMA/ GO2a

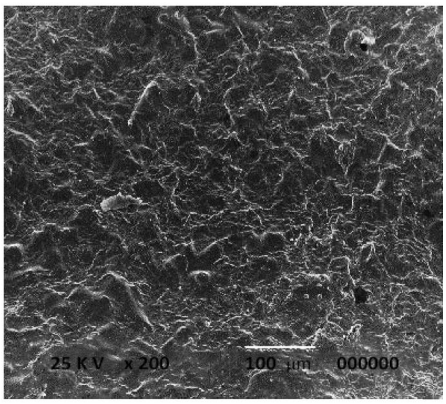

(c) ST-PHEMA/ GO2c

Fig. 3 SEM micrograph of: (**a**) ST-PHEMAc hydrogel, **b** ST-PHEMA/GO2a & **c** ST-PHEMA/GO2c nanocomposite hydrogel (×200) nanocomposite hydrogels

2D and 3D images for GO in addition to AFM images for ST-PHEMAc, ST-PHEMA/GO2a and ST-PHEMA/GO2c are shown in Fig. 4 a–f, respectively. The images of graphene oxide depict lowest height (5.78 nm) and highest roughness (38.11 nm). Upon formin the hydrogels, the height increases from 6.9 nm to 25.6 nm for ST-PHEMAc and ST-PHEMA/GO2c, respectively. On the other hand, the roughness values of all the hydrogel nanocomposites are much smaller than the roughness measurement of GO. The images reveal the same surface features observed by the SEM. Image Fig. 4a (ST-PHEMAc) shows smooth surface with very low height (6.9 nm), whereas images 4b and 4c show rough surface due to the incorporation of graphene oxide nanoparticles. It is also clear that both the height and the roughness increase as the irradiation dose increases from 10 to 30 kGy (ST-PHEMA/GO2a and ST-PHEMA/GO2c) amount of graphene oxide rises, all the data are tabulated in Table 3. Furthermore, the distribution pattern of the graphene oxide nanoparticles is very clear in both images and confirm that fabrication process is performed successfully (Hasan et al. 2022).

Transmission electron microscopy (TEM)

TEM images of ST-PHEMAc hydrogel, ST-PHEMA/GO2a and ST-PHEMA/GO2c nanocomposite hydrogels are presented in Fig. 5. Both dark lines and grey regions demonstrated GO sheets as well as ST-PHEMA polymeric matrix. GO sheets exist uniformly dispersed as exfoliated sheets in ST-PHEMA polymeric matrix. The average size of both ST-PHEMA/GO2a and ST-PHEMA/GO2c nanocomposite hydrogels is around 19.8 to 41.3 nm. The wrinkled sheets inhibit GO agglomeration originated from van der Waals forces during the drying process.

Swelling behavior analysis

Swelling behavior assessment of hydrogel compounds is a vital element because of using these hydrogels in different implementations, comprising drug delivery as well as tissue engineering (Graham and McNeill 1984; Caccavo et al. 2016; Bettini et al. 1994). Hydrogel swelling behavior is

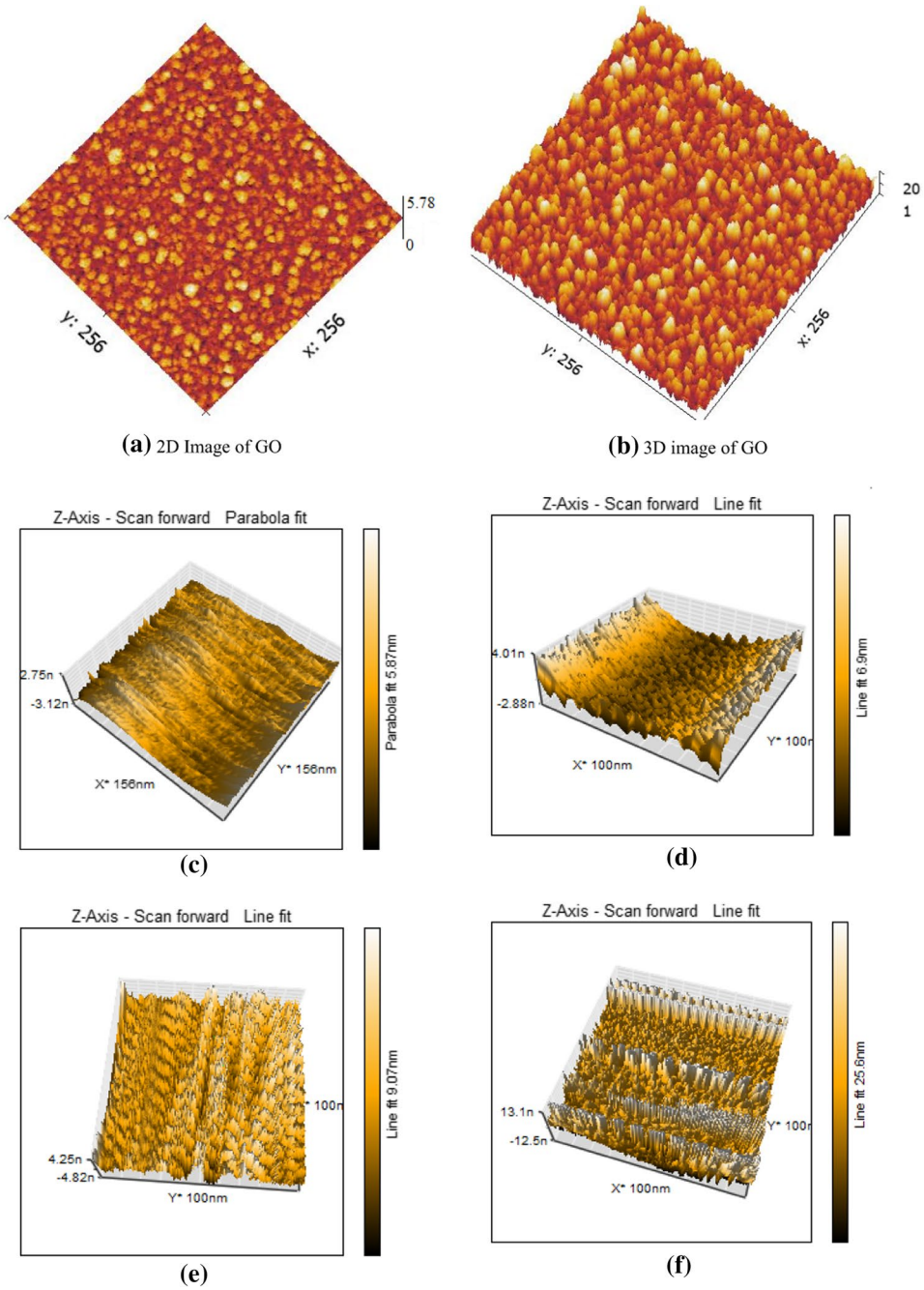

Fig. 4 AFM images of (**a**) 2D image of graphene oxide **b** 3D image of GO, **c** ST-PHEMAc **d** ST-PHEMAc, **e** ST-PHEMA-GO2a, and **f** ST-PHEMAGO2c

Table 3 AFM data for some samples

No	Sample	Height	Data analysis	R_a (average roughness)
1	GO	5.78 nm	parabola	38.11 nm
2	ST-HEMAc	6.9 nm	Line fit	11.04 nm
3	ST-PHEMA/GO2a	9.07 nm	Line fit	11.15 nm
4	ST-PHEMA/GO2c	25.6 nm	Line fit	24.41 nm

a crucial feature for its drug delivery mechanism (Parent et al. 2017).

Swelling performance versus time

Figure 6 a, b show the dynamic swelling behavior of ST-PHEMA hydrogel and ST-PHEMA/ GO nanocomposites in distilled water. The swelling behavior of ST-PHEMAGO2 nanocomposite hydrogel with different irradiation doses of 10, 20, and 30 kGy was evaluated at different time intervals in deionized water.

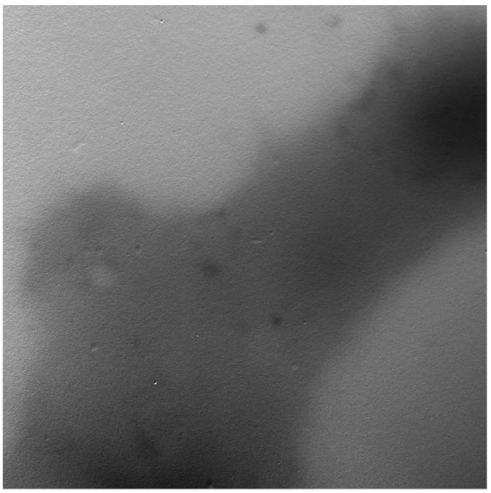

(a) ST-PHEMAc

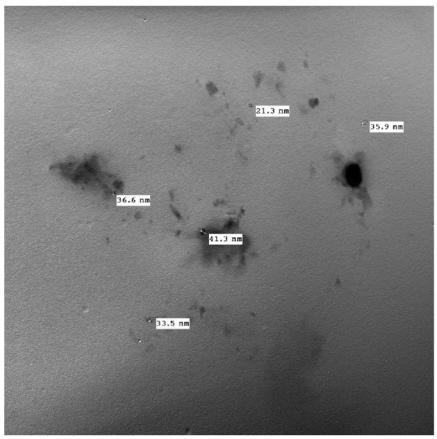

(b) ST-PHEMA/GO2a

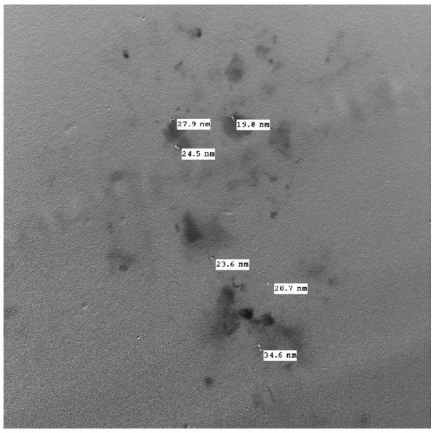

(c) ST-PHEMA/GO2c

Fig. 5 TEM micrograph of: (**a**) ST-PHEMAc hydrogel; **b** ST-PHEMA/GO2a & **c** ST-PHEMA/GO2c nanocomposite hydrogel; Print Mag: 63000x@211 mm; Direct Mag:3000x

As shown in Fig. 6a, b for all curves, the swelling performance is enhanced rapidly by time then the rate decreases until reaching the stationary phase (maximum constant content after 3 h). As GO content increases, the equilibrium swelling (g g^{-1}) decreases (110.5, 106.4, and 98.7 wt% for ST-HEMAc, ST-PHEMA/GO1c, and ST-PHEMA/GO2c, respectively). This behavior may be attributed to that the increase of graphene oxide content may cause an intensified crosslinking and obvious reduction in pore size (Fig. 6a). Furthermore, the flexibility of polymeric chains was considerably restricted by excess GO content in crosslinked networks, fixing polymer ability to produce hydrogen bonds and reduce water absorption (Chen et al. 2019).

As depicted in Fig. 6b, by increasing irradiation dose of ST-PHEMA/GO nanocomposites, the swelling percentage (wt%) was found 128.3, 112.9, and 98.7 at 10, 20, and 30 kGy, respectively. With a subsequent increase in irradiation dose, the crosslinking density augments, and the hydrogel becomes more tightly packed, leading to decrease water diffusion through the polymeric matrix (Wasikiewicz et al. 2006).

Effect of pH on swelling capacity

The pH of the solution is a primary factor that impacts the drug carrier process through controlling the electrostatic interaction between adsorbent surface and ions existing in the reaction medium. (Parent et al. 2017). The ST-PHEMA hydrogel comprising hydrophilic moieties get protonated in an acidic medium, resulting in intermolecular H-bonding; consequently, equilibrium swelling percentage decreases (Fig. 6c, d). Therefore, extra physical crosslinking through H-bonding formation happened, minimizing water uptake.

In contrast, equilibrium swelling percentage is higher in basic medium as hydrophilic groups in hydrogel network are being deprotonated, leading to intermolecular H-bonds with water molecules and swelling percentage increase.

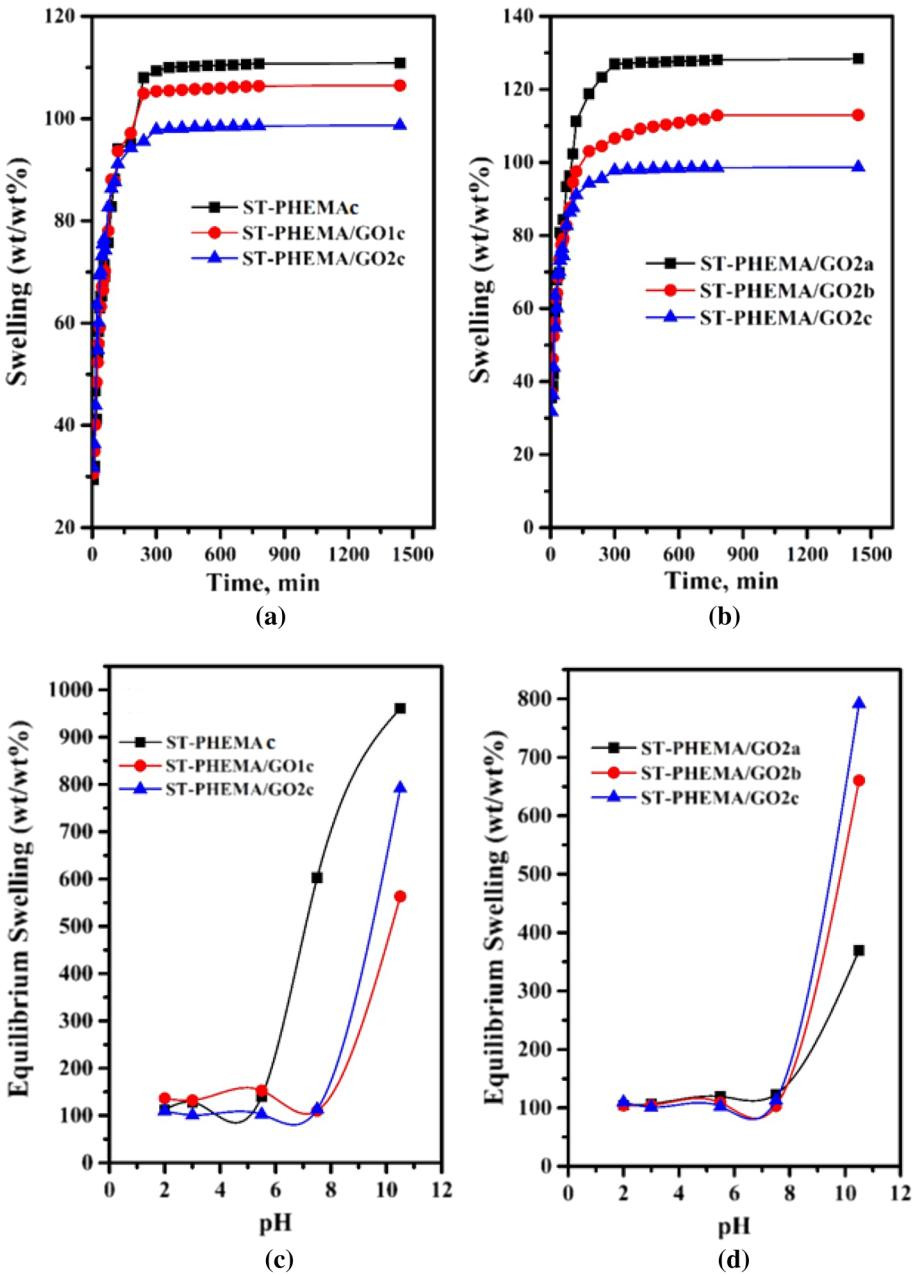

Fig. 6 **a** Swelling percent at different time interval for ST-HEMAc hydrogel, ST-PHEMA/GO1c & ST-PHEMA/GO2c, nanocomposite hydrogels. **b** Swelling percentage at different time interval for ST-PHEMA/GO2a; ST-PHEMA/GO2b & ST-PHEMA/GO2c hydrogel nanocomposite **c** equilibrium swelling percentage as function of pH for ST-HEMAc hydrogel, and ST-HEMA/GO1c & ST-HEMA/GO2c, nanocomposite hydrogels **d** equilibrium swelling percentage as function of pH for ST-HEMA/GO2a; ST-HEMA/GO2b & ST-HEMA/GO2c nanocomposite hydrogel

Swelling kinetics

In this study, water intake was observed through swelling ratio determination of hydrogel at desired time intervals as described earlier.

The swelling behavior of hydrogels is complicated as their swelling process is splitted into three successive stages. In the initial stage, gel material is dry with multiple voids, and swelling happens when the water crosses the gel threshold through the pores capillary phenomenon via association with hydrophilic gel groups (He et al. 2019). After that, the gel pores retain sufficient water, and the hydrophilic gel groups as well as water particles associated to access the gel network structure, causing relaxation and swelling of the gel polymer chains. Eventually, the gel reaches the swelling equilibrium state as the network structure swells completely with extending the bound polymer chains in water due to the gel fully swollen.

Fick's law Eqs. (4 and 5) are a phenomenological rate law where "n" helps in the identification of the water-sorption mechanism type in operation. For instance, the sorption process is diffusion-controlled when n less than 0.5 as it shows Fickian kinetics, while non-Fickian process and chain relaxation affecting the water-sorption process is indicated when a value of n between 0.5 and 1.0.

The values of "n" of the prepared nanocomposite hydrogel are shown in Fig. 7 and Table 4. The results indicate that water uptake by ST-HEMA hydrogel and ST-HEMA/GO nanocomposite hydrogel follows a Fickian diffusion mechanism for ST-HEMAc, ST-PHEMA/GO1c and ST-PHEMA/GO2c When we studied the effect of irradiation dose, it was found that, at irradiation doses 10 & 20 of ST-HEMA/GO nanocomposites, ST-PHEMA/GO2a, ST-PHEMA/GO2b and ST-PHEMA/GO2c, the sorption also is diffusion-controlled ($n < 0.5$).

Table 4 manifests that water uptake followed the Fickian diffusion mechanism for ST-PHEMAc; hydrogel, ST-PHEMA/GO1c and ST-PHEMA/GO2c nanocomposites as the diffusion exponent (n) ranges from 0.28781 to 0.36378 at the studied condition of irradiation doses 10, 20, and 30 kGy for ST-PHEMA/GO2a, ST-PHEMA/GO2b and ST-PHEMA/GO2c and the swelling rate coefficient, k_s, of ST-PHEMA/GO2c is higher than that of ST-PHEMAc and ST-PHEMA/GO1c at irradiation dose 30 kGy. Moreover, the swelling rate of water absorption (K) is inversely proportional to GO content in the composite gel due to the crosslinking interaction between GO within the polymer matrix and the polymer chains, making gel structure in a lamellar form and decreasing the pore diameter, thus resisting the water diffusion to the gel by reducing the hydrogel capillary. This phenomenon diminishes the water penetration into the polymer matrix (De France et al. 2017).

Table 4 The swelling kinetic parameters of ST-PHEMA hydrogel and ST-PHEMA GO; nanocomposite

Sample	k_s	n	$D \times 10^{-7}$ (cm^2/sec)	K
ST-PHEMAc	0.16865	0.36378	2.37064	0.02764
ST-PHEMA/GO1c	0.16754	0.36076	2.39857	0.02294
ST-PHEMA/GO2a	0.22980	0.29449	2.98772	0.01933
	0.23097	0.28781	1.75648	0.01826
ST-PHEMA/GO2b	0.20718	0.32991	2.00633	0.02366
ST-PHEMA/GO2c				

k_s swelling rate coefficient, n Diffusion exponent, D Diffusion coefficient, K Sorption rate constant

Conclusions

During this study, eco-friendly hydrogel nanocomposites (ST-HEMA/GO) were synthesized by radiation-induced polymerization/crosslinking. The prepared hydrogels were characterized by using FTIR, SEM, AFM, TEM and XRD. The results showed that the distribution of GO within ST-PHEMA matrix becomes more homogeneous as irradiation dose increases and the best distribution is achieved at 30 kGy. TEM and SEM analyses confirmed the presence of GO in polymer matrix in the nanoscale. The AFM data reveal that the roughness increases by increasing the irradiation dose in the polymer matrix and the topographical features indicate the inclusion of GO nanoparticles. The XRD data reveal that the crystallinity of the starch is reduced

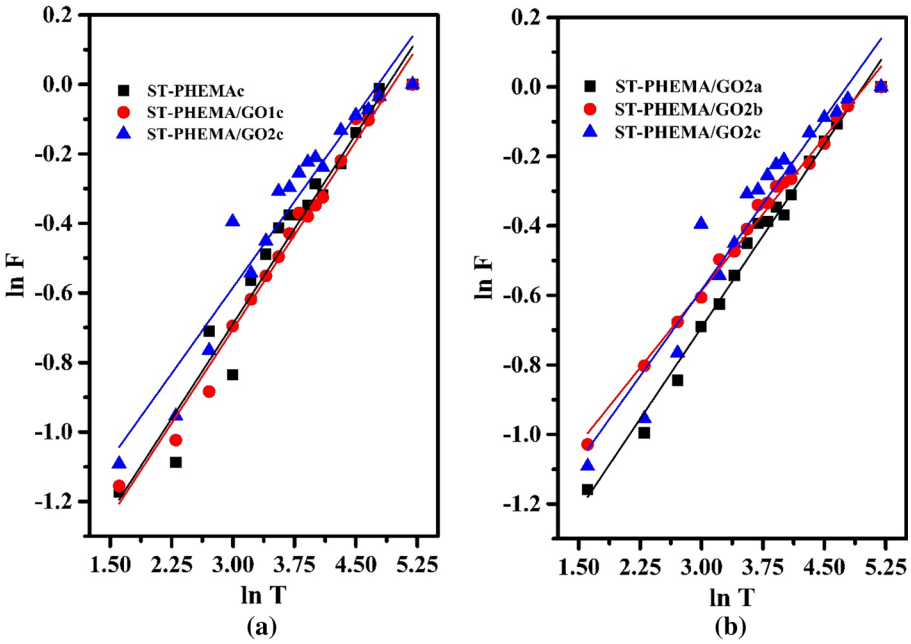

Fig. 7 ln Release fraction versus ln time for **a** ST-PHEMAc, ST-PHEMA/GO1c and ST-PHEMA/GO2c nanocomposite hydrogels, **b** ST-PHEMA/GO2a; ST-HEMA/GO2b & ST-PHEMA/GO2c nanocomposite hydrogel

when forming hydrogels with PHEMA but there are three diffraction peaks in the hydrogel nanocomposites. In addition, the swelling analysis was conducted to investigate the ability of the claimed nanocomposites to act as a vehicle for sustained release application. Furthermore, the higher the GO content, the lower the swelling percentage, and the diffusion exponent (n) according to Fickian law is less than 0.5, indicating that the nanocarrier follows a diffusion-controlled process (Fickian diffusion mechanism). The data also depicted that the swelling capacity is diminished at acidic pH due to protonation of acidic moieties.

Funding Open access funding provided by The Science, Technology & Innovation Funding Authority (STDF) in cooperation with The Egyptian Knowledge Bank (EKB). The authors declare that they have no known competing financial interests or personal relationships that could have appeared to influence the work reported in this paper.

Declarations

Conflict of interest On behalf of all authors, the corresponding author states that there is no conflict of interest.

References

Abbasi F, Mirzadeh H, Katbab AA (2002) Sequential interpenetrating polymer networks of poly (2-hydroxyethyl methacrylate) and polydimethylsiloxane. J Appl Polym Sci 85(9):1825–1831

Abbasian M, Roudi M-M, Mahmoodzadeh F, Eskandani M, Jaymand M (2018) Chitosan-grafted-poly(methacrylic acid)/graphene oxide nanocomposite as a pH-responsive de novo cancer chemotherapy nanosystem. Int J Biol Macromol 118:1871–1879. https://doi.org/10.1016/j.ijbiomac.2018.07.036

Abednejad A, Ghaee A, Morais ES, Sharma M, Neves BM, Freire MG, Nourmohammadi J, Mehrizi AA (2019) Polyvinylidene fluoride-hyaluronic acid wound dressing comprised of ionic liquids for controlled drug delivery and dual therapeutic behavior. Acta Biomater 100:142–157. https://doi.org/10.1016/j.actbio.2019.10.007

Ali NH, Amin MCIM, Ng S-F (2019) Sodium carboxymethyl cellulose hydrogels containing reduced graphene oxide (rGO) as a functional antibiofilm wound dressing. J Biomater Sci Polym Ed 30(8):629–645. https://doi.org/10.1080/09205063.2019.1595892

Ansari M, Meftahizadeh H, Eslami H (2021) Fabrication of multifunctional chitosan-guar-aloe vera gel to promote wound healing. Chem Pap. https://doi.org/10.1007/s11696-021-01958-4

Arican F, Uzuner-Demir A, Sancakli A, Ismar E (2021) Synthesis and characterization of superabsorbent hydrogels from waste bovine hair via keratin hydrolysate graft with acrylic acid (AA) and acrylamide (AAm). Chem Pap 75(12):6601–6610. https://doi.org/10.1007/s11696-021-01828-z

Arshad F, Selvaraj M, Zain J, Banat F, Haija MA (2019) Polyethylenimine modified graphene oxide hydrogel composite as an efficient adsorbent for heavy metal ions. Sep Purif Technol 209:870–880. https://doi.org/10.1016/j.seppur.2018.06.035

Basiak E, Lenart A, Debeaufort F (2018) How glycerol and water contents affect the structural and functional properties of starch-based edible films. Polymers 10:412. https://doi.org/10.3390/polym10040412

Bettini R, Colombo P, Massimo G, Catellani PL, Vitali T (1994) Swelling and drug release in hydrogel matrices: polymer viscosity and matrix porosity effects. Eur J Pharm Sci 2(3):213–219

Bhattacharyya R, Ray SK (2014) Enhanced adsorption of synthetic dyes from aqueous solution by a semi-interpenetrating network hydrogel based on starch. J Ind Eng Chem 20(5):3714–3725. https://doi.org/10.1016/j.jiec.2013.12.071

Caccavo D, Cascone S, Gaetano L, Barba AA, Larsson A (2016) Swellable hydrogel-based systems for controlled drug delivery. In: Sezer AD (ed) Smart drug delivery system. In tech, pp 237–303

Chen H-H, Shi-Ying Xu, Wang Z (2006) Gelation properties of flaxseed gum. J Food Eng 77(2):295–303

Chen W, Xiao P, Chen H, Zhang H, Zhang Q, Chen Y (2019) Polymeric graphene bulk materials with a 3D cross-linked monolithic graphene network. Adv Mater 31(9):1802403

Chin SF, Romainor ANB, Pang SC, Lihan S (2019) Antimicrobial starch-citrate hydrogel for potential applications as drug delivery carriers. J Drug Deliv Sci Technol 54:101239. https://doi.org/10.1016/j.jddst.2019.101239

Fares MM, El-faqeeh AS, Osman ME (2003) Graft copolymerization onto starch–i synthesis and optimization of starch grafted with n-tert-butylacrylamide copolymer and its hydrogels. J Polym Res 10(2):119–125. https://doi.org/10.1023/A:1024928722345

France De, Kevin J, Hoare T, Cranston ED (2017) Review of hydrogels and aerogels containing nanocellulose. Chem Mater 29(11):4609–4631

Ganguly S, Maity T, Mondal S, Das P, Das NC (2017) Starch functionalized biodegradable semi-IPN as a pH-tunable controlled release platform for memantine. Int J Biol Macromol 95:185–198

Graham NB, McNeill ME (1984) Hydrogels for controlled drug delivery. Biomaterials 5(1):27–36. https://doi.org/10.1016/0142-9612(84)90063-2

Güler MA, Gök MK, Figen AK, Özgümüş S (2015) Swelling, mechanical and mucoadhesion properties of Mt/starch-g-PMAA nanocomposite hydrogels. Appl Clay Sci 112–113:44–52. https://doi.org/10.1016/j.clay.2015.04.019

Guo L, Sato H, Hashimoto T, Ozaki Y (2010) FTIR study on hydrogen-bonding interactions in biodegradable polymer blends of poly (3-hydroxybutyrate) and poly (4-vinylphenol). Macromolecules 43(8):3897–3902

Han D, Yan L, Chen W, Li W (2011) Preparation of chitosan/graphene oxide composite film with enhanced mechanical strength in the wet state. Carbohyd Polym 83(2):653–658. https://doi.org/10.1016/j.carbpol.2010.08.038

Haq F, Haojie Yu, Wang Y, Wang Li, Haroon M, Khan A, Mehmood S, Ul AB, Lin T (2020) Synthesis of carboxymethyl starch grafted poly (methacrylic acids) (CMS-g-PMAAs) and their application as an adsorbent for the removal of ammonia and phenol. J Mol Struct 1207:127752. https://doi.org/10.1016/j.molstruc.2020.127752

Hasan AMA, Keshawy M, Abdel-Raouf M-S (2022) Atomic force microscopy investigation of smart superabsorbent hydrogels based

on carboxymethyl guar gum: Surface topography and swelling properties. Mater Chem Phys 278:125521
He F, Zhou Q, Wang L, Gaobo Yu, Li J, Feng Y (2019) Fabrication of a sustained release delivery system for pesticides using interpenetrating polyacrylamide/alginate/montmorillonite nanocomposite hydrogels. Appl Clay Sci 183:105347
Huang T, Zhang L, Chen H, Gao C (2015) A cross-linking graphene oxide–polyethyleneimine hybrid film containing ciprofloxacin: one-step preparation, controlled drug release and antibacterial performance. J Mater Chem B 3(8):1605–1611. https://doi.org/10.1039/C4TB01896F
Ikeda S, Nitta Y, Temsiripong T, Pongsawatmanit R, Nishinari K (2004) Atomic force microscopy studies on cation-induced network formation of gellan. Food Hydrocoll 18(5):727–735
Jeyanthi R, Panduranga K (1990) Collagen-poly (Hema) hydrogels for the controlled release of anticancer drugs—preparation and characterization. J Bioact Compat Polym 5(2):194–211
Jia Wu, Xiao D, Zhang Y, Lan W, Tian B-Q, Xie B-J (2009) Application of atomic force microscopy in the study of polysaccharide. Agric Sci China 8(12):1458–1465
Konstantakos S, Marinopoulou A, Papaemmanouil S, Emmanouilidou M, Karamalaki M, Kolothas E, Saridou E, Papastergiadis E, Karageorgiou V (2019) Preparation of model starch complex hydrogels. Food Hydrocoll 96:365–372. https://doi.org/10.1016/j.foodhyd.2019.05.046
Krishnamoorthy K, Veerapandian M, Yun K, Kim SJ (2013) The chemical and structural analysis of graphene oxide with different degrees of oxidation. Carbon 53:38–49. https://doi.org/10.1016/j.carbon.2012.10.013
Kumar H, Gaur A, Kumar S, Park J-W (2019a) Development of silver nanoparticles-loaded CMC hydrogel using bamboo as a raw material for special medical applications. Chem Pap 73(4):953–964. https://doi.org/10.1007/s11696-018-0650-0
Kumar P, Huo P, Zhang R, Liu Bo (2019b) Antibacterial properties of graphene-based nanomaterials. Nanomater (basel, Switz) 9(5):737. https://doi.org/10.3390/nano9050737
Lanthong P, Nuisin R, Kiatkamjornwong S (2006) Graft copolymerization, characterization, and degradation of cassava starch-g-acrylamide/itaconic acid superabsorbents. Carbohyd Polym 66(2):229–245. https://doi.org/10.1016/j.carbpol.2006.03.006
Liu J, Huang Y, Kumar A, Tan A, Jin S, Mozhi A, Liang X-J (2014) pH-Sensitive nano-systems for drug delivery in cancer therapy. Biotechnol Adv 32(4):693–710. https://doi.org/10.1016/j.biotechadv.2013.11.009
Liu J, Wang X, Yong H, Kan J, Zhang N, Jin C (2018) Preparation, characterization, digestibility and antioxidant activity of quercetin grafted *Cynanchum auriculatum* starch. Int J Biol Macromol 114:130–136. https://doi.org/10.1016/j.ijbiomac.2018.03.101
Mahmoud GA, Abdel-Aal SE, Badway NA, Abo SA, Farha, and Esraa A Alshafei, (2014) Radiation synthesis and characterization of starch-based hydrogels for removal of acid dye. Starch-Stärke 66(3–4):400–408
Maji B (2019) 1 - Introduction to natural polysaccharides. In: Maiti S, Jana S (eds) Functional polysaccharides for biomedical applications. Woodhead Publishing, Sawston, pp 1–31
Mandal B, Ray SK (2015) Synthesis, characterization, swelling and dye adsorption properties of starch incorporated acrylic gels. Int J Biol Macromol 81:847–857. https://doi.org/10.1016/j.ijbiomac.2015.08.050
Miao W, Shim G, Kang CM, Lee S, Choe YS, Choi HG, Oh YK (2013) Cholesteryl hyaluronic acid-coated, reduced graphene oxide nanosheets for anti-cancer drug delivery. Biomaterials 34(37):9638–9647. https://doi.org/10.1016/j.biomaterials.2013.08.058
Mishra RK, Ha SK, Verma K, Tiwari SK (2018) Recent progress in selected bio-nanomaterials and their engineering applications: An overview. J Sci Adv Mater Devices 3(3):263–288. https://doi.org/10.1016/j.jsamd.2018.05.003
Naicker C, Nombona N, Van Zyl WE (2020) Fabrication of novel magnetic chitosan/graphene-oxide/metal oxide nanocomposite beads for Cr (VI) adsorption. Chem Pap 74(2):529–541
Noivoil N, Yoksan R (2020) Oligo(lactic acid)-grafted starch: A compatibilizer for poly(lactic acid)/thermoplastic starch blend. Int J Biol Macromol 160:506–517. https://doi.org/10.1016/j.ijbiomac.2020.05.178
Papageorgiou DG, Kinloch IA, Young RJ (2017) Mechanical properties of graphene and graphene-based nanocomposites. Prog Mater Sci 90:75–127. https://doi.org/10.1016/j.pmatsci.2017.07.004
Parent M, Baradari H, Champion E, Damia C, Viana-Trecant M (2017) Design of calcium phosphate ceramics for drug delivery applications in bone diseases: a review of the parameters affecting the loading and release of the therapeutic substance. J Control Release 252:1–17
Pereira AT, Henriques PC, Costa PC, Maria Cristina L, Martins FD, Magalhães, and Inês C Gonçalves, (2019) Graphene oxide-reinforced poly (2-hydroxyethyl methacrylate) hydrogels with extreme stiffness and high-strength. Compos Sci Technol 184:107819
Qi Y, Cao Y, Meng X, Cao J, Li X, Qingli Hao Wu, Lei QL, Li J, Si W (2019) Facile synthesis of 3D sulfur/nitrogen co-doped graphene derived from graphene oxide hydrogel and the simultaneous determination of hydroquinone and catechol. Sens Actuators, B Chem 279:170–176. https://doi.org/10.1016/j.snb.2018.09.067
Rao Z, Ge H, Liu L, Zhu C, Min L, Liu M, Fan L, Li D (2018) Carboxymethyl cellulose modified graphene oxide as pH-sensitive drug delivery system. Int J Biol Macromol 107(Pt A):1184–1192. https://doi.org/10.1016/j.ijbiomac.2017.09.096
Rasoulzadehzali M, Namazi H (2018) Facile preparation of antibacterial chitosan/graphene oxide-Ag bio-nanocomposite hydrogel beads for controlled release of doxorubicin. Int J Biol Macromol 116:54–63. https://doi.org/10.1016/j.ijbiomac.2018.04.140
Rattanawongwiboon T, Hemvichian K, Lertsarawut P, Suwanmala P (2020) Chitosan-poly (ethylene glycol) diacrylate beads prepared by radiation-induced crosslinking and their promising applications derived from encapsulation of essential oils. Radiat Phys Chem 170:108656
Sadeghi M (2010) Synthesis and swelling behaviors of graftcopolymer based on chitosan-g-poly (AA-co-HEMA). Int J Chem Eng Appl 1(4):354
Saha NK, Balakrishnan M, Ulbricht M (2007) Sugarcane juice ultrafiltration: FTIR and SEM analysis of polysaccharide fouling. J Membr Sci 306(1):287–297. https://doi.org/10.1016/j.memsci.2007.09.006
Sarkar N, Sahoo G, Swain SK (2020) Graphene quantum dot decorated magnetic graphene oxide filled polyvinyl alcohol hybrid hydrogel for removal of dye pollutants. J Mol Liq 302:112591. https://doi.org/10.1016/j.molliq.2020.112591
Satish CS, Shivakumar HG (2007) Formulation and evaluation of self-regulated insulin delivery system based on poly (HEMA-co-DMAEMA) hydrogels. J Macromol Sci Part A Pure Appl Chem 44(4):379–387
Sayed A, Mahmoud GA, Said H, Diab AA (2022) Characterization and optimization of magnetic Gum-PVP/SiO2 nanocomposite hydrogel for removal of contaminated dyes. Mater Chem Phys 280:125731. https://doi.org/10.1016/j.matchemphys.2022.125731
Shirin R, Hamid M, Hamid M, Esmaeil MM (2019) A review on nanocomposite hydrogels and their biomedical applications. Sci Eng Compos Mater 26(1):154–174. https://doi.org/10.1515/secm-2017-0161
Singh B, Singh B (2020) Radiation induced graft copolymerization of graphene oxide and carbopol onto sterculia gum polysaccharide to develop hydrogels for biomedical applications. FlatChem 19:100151. https://doi.org/10.1016/j.flatc.2019.100151

Sivakumar M, Panduranga Rao K (2002) Synthesis, characterization, and in vitro release of ibuprofen from poly (MMA-HEMA) copolymeric core–shell hydrogel microspheres for biomedical applications. J Appl Polym Sci 83(14):3045–3054

Subedi N, Lähde A, Abu-Danso E, Iqbal J, Bhatnagar A (2019) A comparative study of magnetic chitosan (Chi@ Fe3O4) and graphene oxide modified magnetic chitosan (Chi@ Fe3O4GO) nanocomposites for efficient removal of Cr (VI) from water. Int J Biol Macromol 137:948–959

Todica M (2015) Spectroscopic investigation of gamma irradiated PAA-graphite membranes. Indian J Pure Appl Phys (IJPAP) 53(6):359–366

Wang T, Xueyan Mu, Li H, Weilong Wu, Nie J, Yang D (2013) The photocrosslinkable tissue adhesive based on copolymeric dextran/HEMA. Carbohyd Polym 92(2):1423–1431

Wasikiewicz JM, Mitomo H, Nagasawa N, Yagi T, Tamada M, Yoshii F (2006) Radiation crosslinking of biodegradable carboxymethylchitin and carboxymethylchitosan. J Appl Polym Sci 102(1):758–767

Weerapoprasit C, Prachayawarakorn J (2019) Characterization and properties of biodegradable thermoplastic grafted starch films by different contents of methacrylic acid. Int J Biol Macromol 123:657–663. https://doi.org/10.1016/j.ijbiomac.2018.11.083

Wöhl-Bruhn S, Bertz A, Harling S, Menzel H, Bunjes H (2012) Hydroxyethyl starch-based polymers for the controlled release of biomacromolecules from hydrogel microspheres. Eur J Pharm Biopharm 81(3):573–581. https://doi.org/10.1016/j.ejpb.2012.04.017

Xie J, Huang L, Wang R, Ye S, Song X (2020) Novel visible light-responsive graphene oxide/Bi2WO6/starch composite membrane for efficient degradation of ethylene. Carbohyd Polym 246:116640. https://doi.org/10.1016/j.carbpol.2020.116640

Yang S, Lei P, Shan Y, Zhang D (2018) Preparation and characterization of antibacterial electrospun chitosan/poly (vinyl alcohol)/graphene oxide composite nanofibrous membrane. Appl Surf Sci 435:832–840. https://doi.org/10.1016/j.apsusc.2017.11.191

Yu Y, Wang Y-N, Ding W, Zhou J, Shi Bi (2017) Preparation of highly-oxidized starch using hydrogen peroxide and its application as a novel ligand for zirconium tanning of leather. Carbohyd Polym 174:823–829

Authors and Affiliations

Asmaa Sayed[1] · Mai Yasser[2] · Manar El-sayed Abdel-raouf[3] · Reham Mohsen[2,4]

[1] Polymer Chemistry Department, National Center for Radiation Research and Technology, Egyptian Atomic Energy Authority, Nasr City, Cairo, Egypt

[2] Faculty of Biotechnology, October University for Modern Sciences and Arts (MSA), 6th of October City, Giza, Egypt

[3] Egyptian Petroleum Research Institute, 1 Ahmed Elzomor street, Nasr City 11727, Cairo, Egypt

[4] Faculty of Engineering and Science, University of Greenwich, Medway Campus, Chatham 7 Maritime, Kent ME4 4TB, UK